Journal of Chromatography A, 1218 (2011) 5195–5204

Contents lists available at ScienceDirect

Journal of Chromatography A

journal homepage: www.elsevier.com/locate/chroma

Model simulation and experimental verification of a cation-exchange IgG capture step in batch and continuous chromatography

T. Müller-Späth[a,b], G. Ströhlein[a,b], L. Aumann[a,b], H. Kornmann[c], P. Valax[d], L. Delegrange[d], E. Charbaut[c], G. Baer[d], A. Lamproye[d], M. Jöhnck[e], M. Schulte[e], M. Morbidelli[a,*]

[a] Institute for Chemical and Bioengineering, ETH Zurich, CH-8093 Zurich, Switzerland
[b] ChromaCon AG, Technoparkstr. 1, CH-8005 Zurich, Switzerland
[c] Merck Serono S.A., Zone Industrielle l'Ouriettaz, CH-1170 Aubonne, Switzerland
[d] Merck Serono S.A., Zone Industrielle B, CH-1809 Fenil-sur-Corsier, Switzerland
[e] Merck KGaA, Performance & Life Science Chemicals Research & Development – Life Science, Frankfurter Str. 250, D-64293 Darmstadt, Germany

ARTICLE INFO

Article history:
Received 24 February 2011
Received in revised form 24 May 2011
Accepted 30 May 2011
Available online 12 June 2011

Keywords:
Lumped kinetic model
Monoclonal antibody
Continuous chromatography
MCSGP

ABSTRACT

The cation-exchange capture step of a monoclonal antibody (mAb) purification process using single column batch and multicolumn continuous chromatography (MCSGP) was modeled with a lumped kinetic model. Model parameters were experimentally determined under analytical and preparative conditions: porosities, retention factors and mass transfer parameters of purified mAb were obtained through a systematic procedure based on retention time measurements. The saturation capacity was determined through peak fitting assuming a Langmuir-type adsorption isotherm. The model was validated using linear batch gradient elutions. In addition, the model was used to simulate the start-up, cyclic steady state and shut down behavior of the continuous capture process (MCSGP) and to predict performance parameters. The obtained results were validated by comparison with suitable experiments using an industrial cell culture supernatant. Although the model was not capable of delivering quantitative information of the product purity, it proved high accuracy in the prediction of product concentrations and yield with an error of less than 6%, making it a very useful tool in process development.

1. Introduction

Monoclonal antibodies (mAbs) and antibody-related proteins have been developed and approved in increasing numbers in the last two decades [1] and have reached sales in the billion-$ scale [2].

With advancing cell line optimization mAb can be produced in cell culture with titers exceeding 5 g/L [3]. Throughout the industry a purification platform based on protein A affinity chromatography is established, followed usually by one or two chromatographic polishing steps [3,4].

Although protein A chromatography represents a very effective method to clear major impurities such as host cell proteins (HCPs), it has some disadvantages such as relatively high stationary phase costs and limited cleanability with caustic soda. Protein A stationary phase costs and lifetime are a dominant factor in economic calculations with respect to downstream processing [4]. As replacement for protein A chromatography, mainly cation-exchange chromatography has been investigated. Cation-exchange chromatography as capture step in mAb purification has been described in single column batch mode [5–10] and in continuous mode [7,10] by various authors. The combination of a precipitation method and cation exchange chromatography proved very effective for HCP reduction and was used instead of the affinity chromatography capture step [11,12].

In this work the modeling of a cation exchange capture step is outlined. The goal was to describe the performance of a capture step using single column batch chromatography and continuous chromatography (MCSGP) in terms of product yield and productivity using the same model.

Previous modeling work related to preparative ion exchange chromatography of monoclonal antibodies has focused on investigating the influence of mobile and stationary phase parameters, such as the ionic strength (mobile phase) and the ligand density (stationary phase) on mass transfer and adsorption equilibrium of the target product. The fact that mAbs are large complex molecules comprising many charged and hydrophobic patches that inter-

* Corresponding author at: Institute for Chemical and Bioengineering, ETH Zurich, Wolfgang-Pauli-Str. 10/HCI F 129, 8093 Zurich, Switzerland.
Tel.: +41 44 6323034/6323033; fax: +41 44 6321082.
E-mail address: massimo.morbidelli@chem.ethz.ch (M. Morbidelli).
URL: http://www.morbidelli.ethz.ch (M. Morbidelli).

0021-9673/$ – see front matter © 2011 Elsevier B.V. All rights reserved.
doi:10.1016/j.chroma.2011.05.103

act with the stationary phase and change with the mobile phase composition complicates the development of a precise analytical model. Significant efforts have been made in determining molecule structure–adsorption relationships in ion exchange chromatography [13], also with the aim of a priori prediction of adsorption behavior of proteins [14,15]. Adsorption equilibria for large proteins are established slowly due to diffusion limitation [16,17], electrostatic effects [18,19] and conformational changes on a pore level.

Most frequently, the adsorption equilibrium is described using a competitive Langmuir model [20,21] or a steric mass action model [22,23].

In order to account for diffusional limitations, the adsorption equilibrium models are frequently combined with pore or general rate models including competition of the proteins [20,21,24].

The separation of model proteins on cation exchange stationary phases under gradient conditions has been described by various authors using the above mentioned adsorption equilibria models, e.g. by Forrer et al., Voitl et al. and Orellana et al. [20,21,25] and Gallant et al. [23], respectively. The optimization of a model protein purification using cation exchange gradient chromatography was described by Degerman et al. [26] based on the general rate model.

Despite the complexity of the protein adsorption and diffusion kinetics, lumped kinetic models combining the contributions of mass transfer and diffusional resistances within a single mass transfer parameter and using a linear driving force approximation have proven practical to describe single column batch chromatography gradient processes [27,28].

All models rely on a number of parameters that need to be determined experimentally, since a priori prediction is not accurate enough for complex molecules such as mAbs. An overview of different methods of adsorption equilibrium parameter determination has been provided by Seidel-Morgenstern [29]. A comprehensive summary of methods applied to determine mass transfer parameters in cation exchange chromatography has been presented along with modeling aspects by Carta et al. [30].

In this work, an experimental procedure for acquisition of model parameters for a lumped kinetic model with linear driving force approximation [27,28] is described for the purification of an industrially relevant mAb. The model is validated using single column batch cation exchange gradient experiments and then used to describe the performance of a multicolumn continuous mAb purification step (MCSGP) in terms of yield and productivity.

Multicolumn countercurrent solvent gradient purification (MCSGP) is a continuous chromatographic process capable of delivering product at high yield and purity simultaneously [31,32]. This feature is due to the process-integrated internal recycling of partially purified side fractions. Since MCSGP separates the feed solution into at least three fractions, it is particularly suited for biopurifications where an intermediate product is flanked by weakly and strongly adsorbing impurities. MCSGP has been successfully applied to various processes e.g. peptide purifications [33], mAb variant separations [34,35] and purification of mAb from cell culture supernatant [10].

Cell culture supernatants represent complex mixtures that are difficult to characterize for instance with respect to HCP behavior. However, modeling is useful for design and required for optimization of chromatographic purification processes for cell culture supernatants. Models and the corresponding parameter evaluation procedure should be proportional to the scope and should account for the complexity of these systems. In other words the level of detail of these models should be proportional to the uncertainty level intrinsic in the characterization of these biological systems.

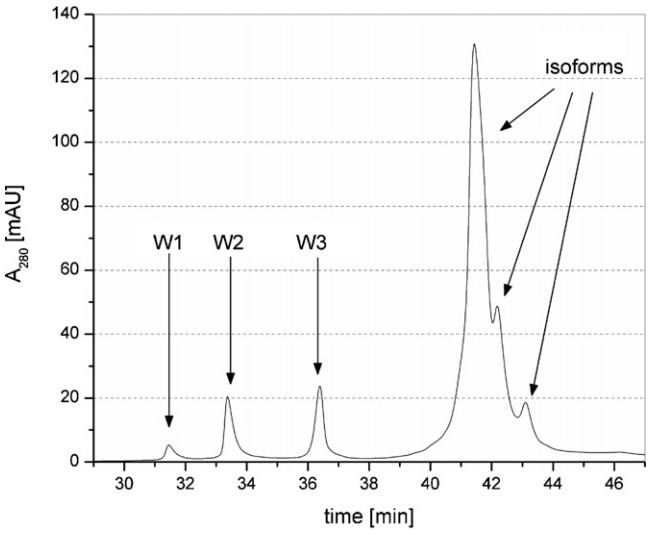

Fig. 1. Gradient elution of cation exchange mAb capture pool, analyzed on a Propac wCX-10 column. The arrows indicate the impurities W1, W2, W3 and the mAb isoforms, respectively.

With this in mind we can develop a very reasonable model and the corresponding parameter evaluation procedure which turns out to be very useful in process design and optimization.

2. Materials and methods

2.1. Monoclonal antibody

Clarified NS0 cell culture supernatant (cCCS) was produced by Merck-Serono (Vevey, Switzerland) and contained IgG_2 with a concentration of $c_{mAb} = 2$ g/L [10]. The conductivity of the cCCS was 16.1 mS/cm and the pH value was 7.25, measured at 25 °C. The host cell protein (HCP) content of the cCCS, determined by ELISA was between 56 000 and 207 000 ppm. The DNA concentration was 8500 ppm and the mAb aggregate content was 4–5%.

In order to ensure binding of the mAb on the cation exchange materials used for capture, feed solutions were prepared by adjusting the pH of the cCCS using acetic acid to pH 5.8 (after dilution of

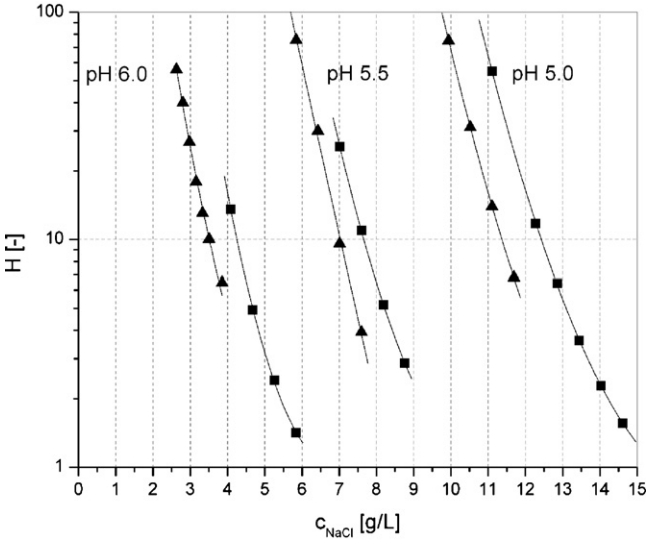

Fig. 2. Henry coefficients as a function of the salt concentration for the stationary phases Poros HS 50 (squares) and Fractogel SO_3 (M) (triangles), measured at different pH values. The lines indicate power function fits, Eq. (8).

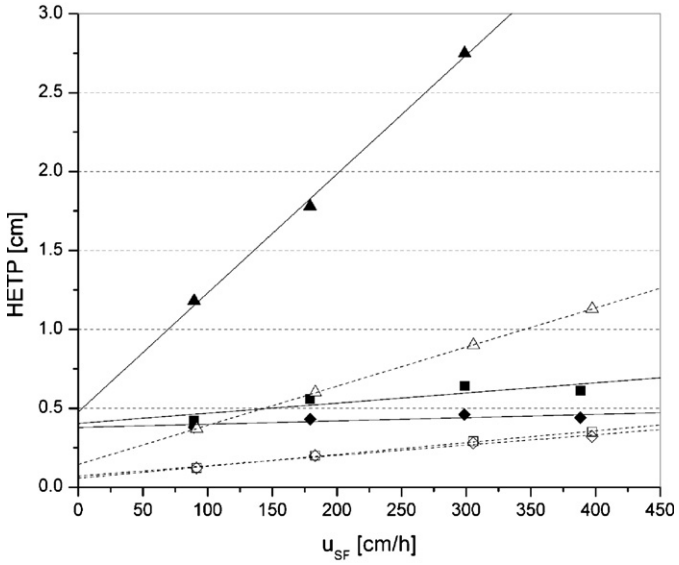

Fig. 3. van Deemter-plot for Fractogel SO_3 (M) (full symbols) and Poros HS 50 (empty symbols) at pH 6.0 and salt concentrations corresponding to 24% B (triangles), 60% B (squares) and 90% B (diamonds).

1:3 with deionized water) or 6.0 (after dilution of 1:4 with deionized water).

For single column batch experiments under overloaded conditions, the feed solution was prepared by concentrating cation-exchange chromatography-purified mAb to 12 g/L and buffer-exchanging through ultrafiltration/diafiltration (UF/DF) with 20 mM phosphate, pH 6.0 (buffer A). Due to the stronger adsorption of the mAb on Poros HS 50 (as a function of the salt concentration) different amounts of diafiltration buffer volumes were used leading to conductivities of the feed of 5.3 mS/cm (Poros HS 50) and 2.3 mS/cm (Fractogel SO_3 (M)) at pH 6.0, respectively.

For retention time measurements of the mAb under isocratic conditions as a function of the pH, feedstocks were prepared from cation-exchange chromatography-purified mAb through UF/DF treatment of with pH 5.0, 5.5 and 6.0 buffers, respectively. For pH 5.0 and 5.5, 20 mM acetate buffers and for pH 6.0, 20 mM phosphate buffers were used, respectively.

2.2. Stationary phases and buffers

For model validation, single column linear gradient elution experiments were carried out using the two cation exchange materials Fractogel SO_3 (M) (Merck, Darmstadt, Germany) and Poros HS 50 (Applied Biosystems, Foster City, CA, USA). Columns and buffer compositions were the same as described in the work by Muller-Spath et al. [10]: the stationary phases had been packed into 0.5 cm × 10 cm Tricorn 5/100 columns (GE Healthcare, Uppsala, Sweden) in the case of Poros HS 50 and 0.75 cm × 10 cm PEEK columns (YMC, Kyoto, Japan) in the case of Fractogel SO_3 (M). The resins had been packed at a linear flow rate of 750 cm/h (Fractogel SO_3 (M)) and 3000 cm/h (Poros HS 50), respectively. For MCSGP four of the above mentioned columns of Fractogel SO_3 (M) and Poros HS 50, respectively, were used. The buffers were: 20 mM phosphate, pH 6.0 (buffer A) as binding and washing buffer; 20 mM phosphate, 0.3 M NaCl, pH 6.0 (buffer B) as elution buffer; 1 M NaOH for cleaning-in-place (CIP) and 500 mM phosphate, 1.0 M NaCl, pH 6.0 as pre-equilibration buffer (for use in MCSGP after CIP). The buffer pH was adjusted using NaOH or phosphoric acid, respectively.

2.3. Preparative chromatography operating conditions

Data from preparative experiments in batch mode (Figs. 4 and 5) and MCSGP mode (Figs. 6–8) was obtained using ÄKTA basic equipment (GE, Uppsala, Sweden), including pumps P-900, UV-900, pH/C-900 and valves PV-908. The conductivity, pH and A_{280} were monitored.

For model validation with the two stationary phases, the following batch capture experiments were carried out in this study:

- Equilibration for 6 min with buffer A at 300 cm/h (3 column volumes).
- Loading for 16 min with feed at 550 cm/h (15 column volumes, Fractogel SO_3 (M))/loading for 14 min with feed at 1000 cm/h (23 column volumes, Poros HS 50).

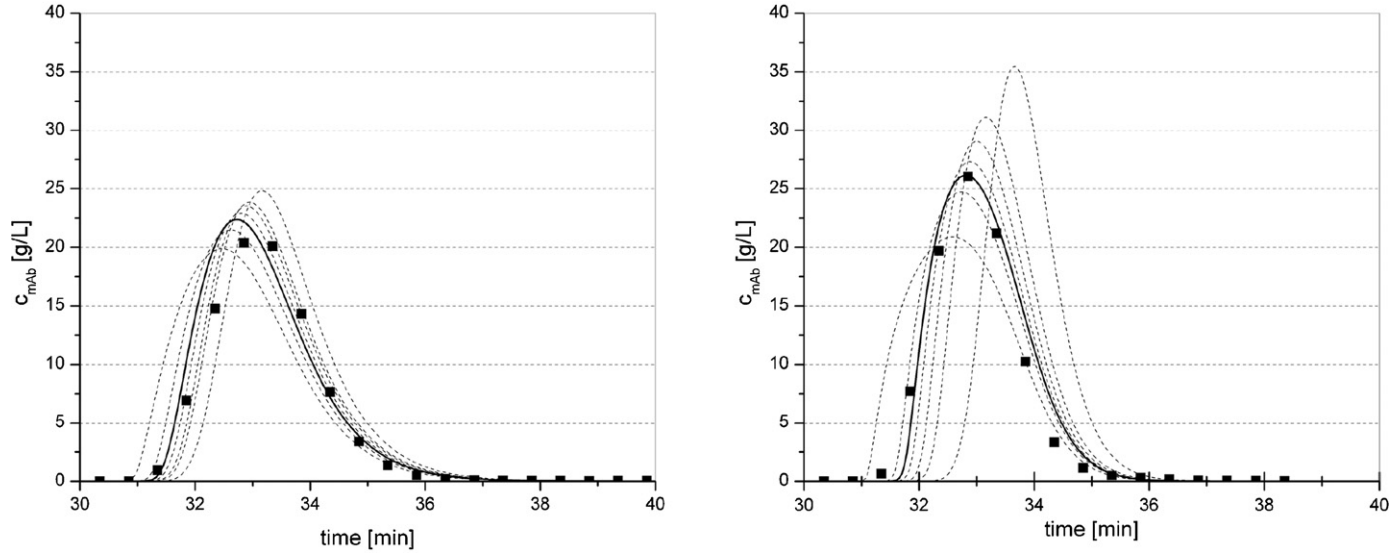

Fig. 4. Gradient elutions for Fractogel SO_3 (M), left, and Poros HS 50, right, under overloaded conditions for peak fitting. The saturation capacity was the only fitting parameter. The lines represent fits with different saturation capacities. In the case of Fractogel these are from highest to lowest curves: linear isotherm (i.e. $q_{Sat} = \infty$), q_{Sat} = 180 g/L, 140 g/L, 120 g/L, 110 g/L, 100 g/L, 80 g/L. For Poros HS 50 these are from highest to lowest curves: linear isotherm (i.e. $q_{Sat} = \infty$), q_{Sat} = 180 g/L, 140 g/L, 120 g/L, 110 g/L, 100 g/L, 80 g/L. The full lines represent the best fits corresponding to q_{Sat} = 120 g/L (Fractogel SO_3 (M)) and q_{Sat} = 110 g/L (Poros HS 50).

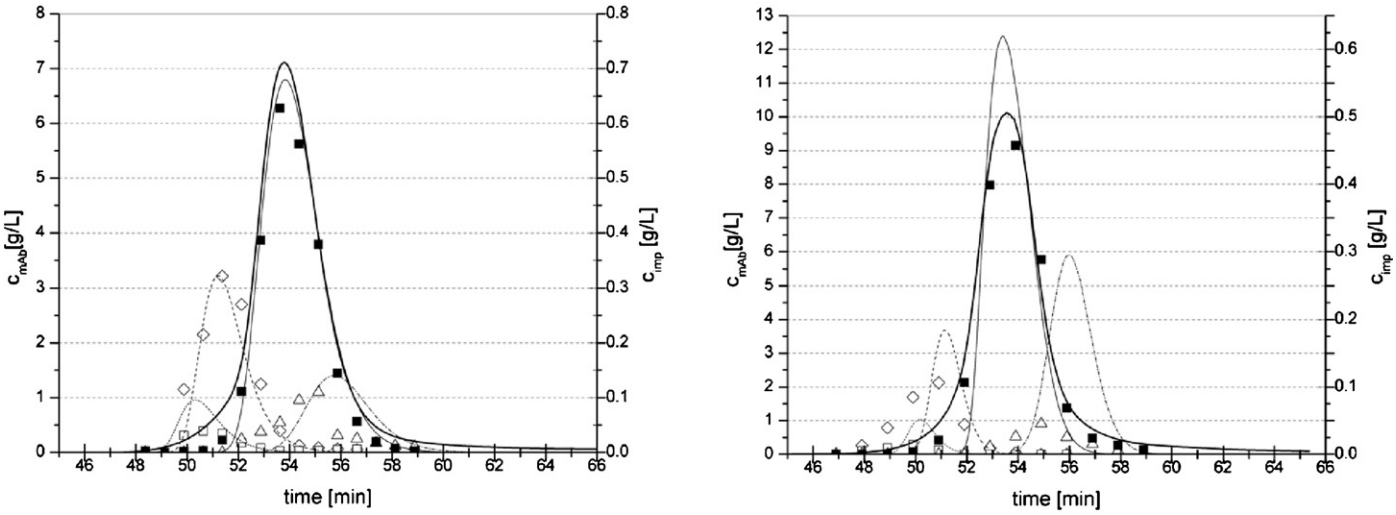

Fig. 5. Batch gradient elution from Fractogel SO_3 (M) (left) and Poros HS 50 (right). The thick solid lines represent the scaled ÄKTA UV-signal at 280 nm. The mAb concentrations (■) were determined offline by analytical protein A chromatography. The thin solid lines indicate the mAb concentration computed by simulation. Symbols: W1 concentrations (□), W2 + W3 concentrations (◊) as determined by Propac analyses. Aggregate concentrations (△) as determined by SEC. The thin dashed lines indicate the simulation results for these three impurities.

- Washing for 20 min with buffer A at 300 cm/h (10 column volumes),
- Elution within 30 min with a gradient from 0 to 100% buffer B at 300 cm/h (15 column volumes),
- Cleaning with 1 M NaOH solution and re-equilibration at 300 cm/h for 10 min (5 column volumes).

Since the linear gradient conditions were the same in this work and in [10] (only the load was different), also the MCSGP operating parameters derived from both sets of experiments were the same. These MCSGP operating parameters served as starting values for the MCSGP simulations shown in this work. The procedure for operating parameter determination is reported by Aumann and Morbidelli [32]. Since the batch gradient chromatograms showed

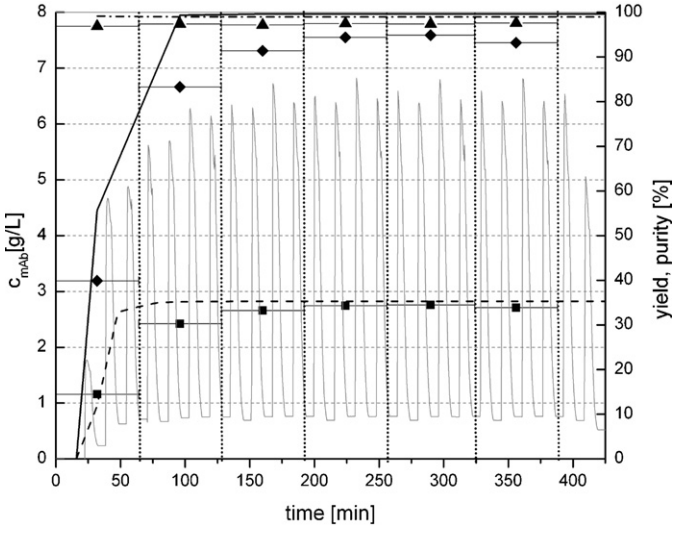

Fig. 6. Comparison of experimental data and simulations of start-up and steady state for run MCSGP 1 (Fractogel SO_3 (M)). The thin grey solid line indicates the A_{280} UV signal recorded at the product outlet as a function of time. The symbols with horizontal bars denote the following parameters calculated from offline measurements (by analytical protein A chromatography) averaged over one cycle: mAb concentration (■, ···), yield (♦, —), purity (▲, -·-·-·). The lines refer to the model simulation results. The vertical lines indicate the sampling intervals that correspond to one cycle.

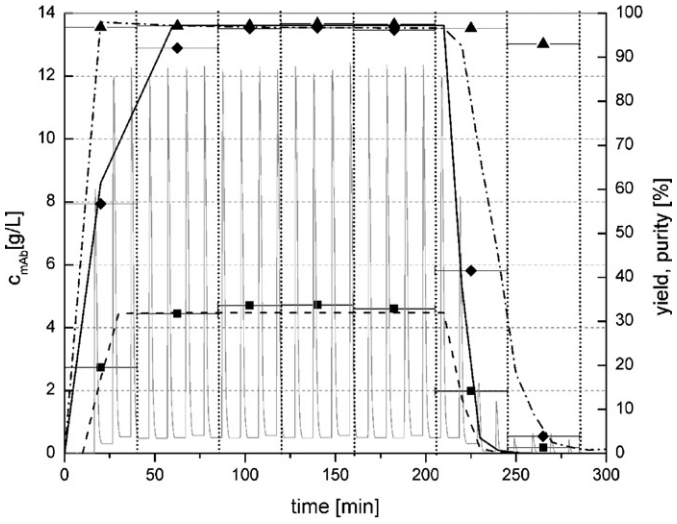

Fig. 7. Start-up, steady state and shutdown for run MCSGP 2 (Poros HS 50). Notation as in Fig. 6.

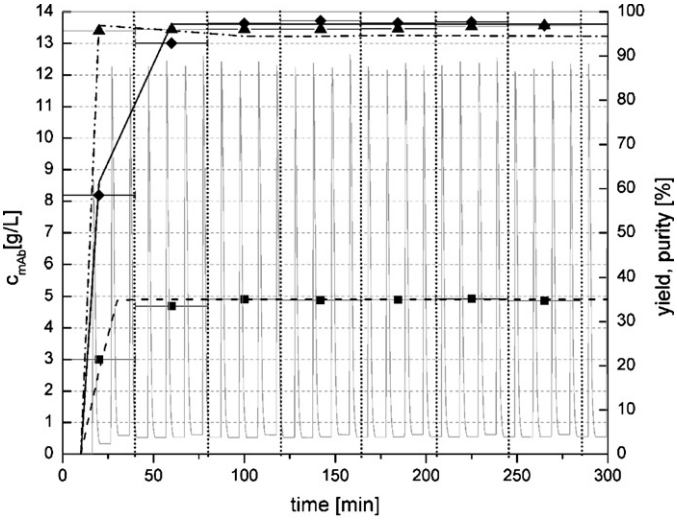

Fig. 8. Start-up and steady state for run MCSGP 3 (Poros HS 50). Notation as in Fig. 6.

very similar retention times of the mAb on Fractogel SO_3 (M) and Poros HS 50 the same starting values could be used for the simulations of MCSGP experiments with these two stationary phases. The MCSGP setup and the experimental runs used for model validation were identical to the ones described in [10].

In order to evaluate the saturation capacities of the investigated stationary phases, experiments under preparative conditions were carried out by loading UF/DF-treated purified mAb onto Fractogel SO_3 (M) and Poros HS 50 columns. The loads were 12 g mAb/L resin (Fractogel SO_3 (M)) and 24 g mAb/L resin (Poros HS 50). The method differed from the chromatography procedure described above only the elution step that comprised a steeper gradient from 0 to 100% buffer B in 15 min in order to reach overloaded conditions. Furthermore the linear flow rate was 300 cm/h in all steps.

2.4. Analytics

The analytical methods used to determine mAb and impurity concentrations included protein A chromatography, analytical weak cation exchange chromatography, size exclusion chromatography (SEC), NS0-HCP-ELISA, SDS polyacrylamide gel electrophoresis and isoelectric focusing for further characterization.

The chromatographic analytics and single column experiments for retention time measurements (data shown in Figs. 1–3) were performed using an Agilent HP 1100 series (Agilent, Santa Clara, CA, USA) at 25 °C with absorption detection at 280 nm.

For mAb quantification, a Poros A/20 analytical protein A column (Applied Biosystems, Foster City, CA, USA) was used. The aggregate content was determined by size exclusion chromatography using a Superdex 200 10/300 column (GE Healthcare, Uppsala, Sweden). Analytical cation exchange chromatography, carried out on Propac wCX-10 4 × 250 mm column (Dionex, Sunnyvale, CA, USA) combined with SDS-PAGE was used to identify three impurities which were closely eluting and weakly adsorbing with respect to the intact mAb and termed W1 (5 kDa impurity), W2 (25 kDa mAb fragment), W3 (50 kDa mAb fragment) according to their elution order [10]. Fig. 1 shows the corresponding analytical chromatogram for a product from a preparative batch ion-exchange purification pool, analyzed with the Propac column. Note that the mAb is present in three charged isoforms.

It was shown that the fragment content in the product pool obtained from batch gradient elutions is strongly dependent on the loading pH ([10], supplemental material section): loading of cCCS of pH 5.5 led to a higher fragment content in the product pool compared to product obtained from a pH 6.0 load, independently of a post-load washing step at pH 6.0 that was expected to equalize the purity. Fragment adsorption as a function of the pH was not included in the model.

Host cell protein (HCP) content was determined by ELISA. Due to their large heterogenity and their low concentrations it is not possible to quantify single HCPs with chromatographic methods. Consequently, HCP adsorption model parameters cannot be determined from chromatographic experiments and the developed model does not include these impurities.

3. Simulation model

3.1. Model development

A lumped kinetic model with linear driving force approximation [27,28] was used to describe the linear batch gradient experiments and the MCSGP process in terms of yield and product concentration. This model is commonly used to describe processes for purification of large molecules such as proteins that display slow mass transfer kinetics when computational time is to be kept low. This aspect is particularly important for the simulation of the cyclic steady state behavior of multicolumn systems such as MCSGP, where peak elutions are occurring permanently. To describe the mass transfer in a detailed manner pore models [24] would be the preferred option but these models require the determination of a larger number of parameters and significantly larger computational time. Lumped kinetic models were found to be a good compromise to describe peak elutions accounting for mass transfer limitations on the one hand and keeping computation time low on the other.

The lumped kinetic model used in this study consists of a mass balance in the mobile phase (Eq. (1)) that accounts also for axial dispersion, a transport equation in the stationary phase (Eq. (2)) and an adsorption equilibrium equation (Eq. (3)).

$$\frac{\partial c_i}{\partial t} + \frac{1-\varepsilon_i}{\varepsilon_i} \cdot \frac{\partial q_i}{\partial t} + u_i \cdot \frac{\partial c_i}{\partial z} = u_i \cdot d_{ax} \frac{\partial^2 c_i}{\partial z^2} \tag{1}$$

$$\frac{\partial q_i}{\partial t} = k_{M,i} \cdot (q_i^* - q_i) \tag{2}$$

$$q^* = \frac{H_i \cdot c_i}{1 + \sum_{i=1}^{n} (H_i / q_{Sat,i}) \cdot c_i} \tag{3}$$

where c_i denotes the concentration of component i in the liquid phase, q_i the concentration in the solid phase and q^* the equilibrium concentration in the solid phase. The component-specific porosity is indicated by ε_i, the Henry coefficient by H_i, the saturation capacity by $q_{Sat,i}$, the component-specific lumped mass transfer coefficient by $k_{M,i}$, the chromatographic flow velocity by u and the axial dispersion coefficient by d_{ax}. The number of modeled components is given by n, which includes the fragment W1, fragments W2 + W3 (lumped), the mAb and aggregates, i.e. $n = 4$.

For the mass transport a linear driving force is assumed, with a constant lumped mass transfer coefficient (Eq. (2)). A Langmuir isotherm including competition of the single components was chosen as adsorption equilibrium model (Eq. (3)). The salt was modeled as fifth adsorbing component using a Langmuir isotherm equation without competition terms. The local liquid phase salt concentration as a function of time was calculated from the imposed gradient conditions (see Section 2.3), Eqs. (1) and (2) and the salt adsorption equilibrium.

The model equations were solved numerically using a 1st order backward finite difference method for the derivatives in space. The model was implemented using Intel Visual Fortran software with IMSL library 5.0. Initial and boundary conditions were chosen according to the experimental conditions. For instance at the beginning of each run, the unit was assumed to be devoid of mAb and impurities, which translates to the following initial conditions:

$$c(z, 0) = 0 \tag{4}$$

The supernatant injection was modeled as a rectangular pulse, giving the boundary condition:

$$\begin{aligned} c(0,t) &= 0 \quad \text{for} \quad t < 0 \\ c(0,t) &= c_{feed} \quad \text{for} \quad 0 < t \le t_p \\ c(0,t) &= 0 \quad \text{for} \quad t_p < t \end{aligned} \tag{5}$$

The MCSGP process was modeled using the same equations and parameters as the single column process. It differed only in the initial and boundary conditions. The MCSGP process includes an interconnected state in which columns are physically connected in order to internally recycle partially purified material. In this case the concentration over time at the inlet of the downstream column is given by the outlet concentration over time of the upstream column (note that a dilution may be performed in between two columns through a pump for adjustment of the modifier concentration).

In MCSGP, the initial local concentration profile, present in each column after the columns have switched positions is given by the final local concentration profile before the switch.

Extra-column dead volumes of the ÄKTA equipment present due to capillaries and connectors were quantified by salt tracer experiments and modeled as plug-flow dead volumes, leading to retardation of the modifier gradients but not to additional mixing.

3.2. Adsorption characterization of the pure mAb

The lumped kinetic model requires the determination of the following parameters for each modeled component *i*: the component-specific porosity ε_i, i.e. the fraction of the column which is accessible to a specific component i, the Henry coefficient H_i, the saturation capacity $q_{Sat,i}$, the lumped mass transfer coefficient $k_{M,i}$, the chromatographic flow velocity u and the axial dispersion coefficient d_{ax}.

The rationale for the adsorption equilibrium boundary parameter determination is to determine the main component (i.e. mAb) parameters as a single component and to assume constant selectivity of the impurities (W1, W2, W3, aggregates), as well as a saturation capacity equal to that of the main components [10]. This procedure is obviously supported by the small relative amounts of the impurities.

The mAb retention behavior is described by the Henry coefficient, which is calculated from the retention time of analytical (i.e. strongly diluted) mAb injections under isocratic conditions and is proportional to the retention factor. The Henry coefficient of a mAb on a given stationary phase is a strong function of the ionic strength of the buffers, their pH value and the temperature.

The retention time of the mAb under isocratic non-adsorbing and adsorbing conditions was measured at pH 5.0, 5.5 and 6.0 in order to determine the porosity and the Henry coefficients of the mAb on Fractogel SO_3 (M) and Poros HS 50 as a function of the pH. For pH 5.0 and 5.5, 20 mM acetate buffers and for pH 6.0, 20 mM phosphate buffers were used. In all cases, the elution buffer contained 1 M NaCl while the binding buffer contained no additional NaCl. The retention times were measured at different concentrations of elution buffer at a linear velocity of 150 cm/h for all columns. All measured retention times were corrected for the equipment dead time. In order to calculate the Henry coefficient, first the mAb-specific porosity $\varepsilon_{\mathrm{mAb}}$ is computed from retention time measurements under non-adsorbing conditions, i.e. high concentrations of elution buffer:

$$\varepsilon_{\mathrm{mAb}} = \frac{t_{0,\mathrm{mAb}} \cdot Q}{V_C} \tag{6}$$

where $t_{0,\mathrm{mAb}}$ denotes the retention time under non-adsorbing conditions, Q the volumetric flow rate and V_C the column volume. It is worth noting that $\varepsilon_{\mathrm{mAb}}$ represents the fraction of pores of the stationary phase which are accessible to the mAb under consideration.

In particular, this porosity value was assumed to be identical for mAb, mAb fragments and mAb aggregates.

Retention time measurements under adsorbing conditions were used to calculate the Henry coefficient of the mAb, H_{mAb}, as a function of the salt concentration, as follows:

$$H_{\mathrm{mAb}} = \left(\frac{t_{R,\mathrm{mAb}}}{t_{0,\mathrm{mAb}}} - 1 \right) \cdot \frac{\varepsilon_{\mathrm{mAb}}}{1 - \varepsilon_{\mathrm{mAb}}} \tag{7}$$

where the term in parentheses is identical to the retention factor k'_{mAb}. The Henry coefficients were fitted with power functions as function of the salt concentration at constant pH for values of pH = 5.0, 5.5 and 6.0, as follows:

$$H_i = \alpha_{1,i} \cdot (c_{\mathrm{NaCl}})^{\alpha_{2,i}} \tag{8}$$

The Henry coefficients H_i, computed using Eq. (8) were used for model validation (see below) to describe adsorption as a function of the local liquid phase salt concentration in the linear salt gradient experiments.

In order to gain information on the mass transfer and the axial dispersion, the retention time of mAb pulse injections and the peak width at half peak height was recorded as a function of the flow velocity (four different flow rates) and the salt concentration at 24%, 60% and 90% B.

The plate height (HETP) for the van Deemter plot was calculated from the following equation [36] using the experimental values of the retention time $t_{R,\mathrm{mAb}}$ and the peak width at half peak height $w_{0.5}$:

$$\mathrm{HETP} = \frac{L}{5.54} \cdot \left(\frac{w_{0.5}}{t_{R,\mathrm{mAb}}} \right)^2 \tag{9}$$

From these data, through fitting with linear functions, van Deemter plots showing HETP over the linear flow velocity u were generated for Fractogel SO_3 (M) and Poros HS 50.

The axial dispersion and the lumped mass transfer coefficient were determined by comparison of the linear functions with the plate height equation (10) introduced by van Deemter [37] which is valid in the linear range of the adsorption isotherm:

$$\mathrm{HETP}(u_{SF}) = \frac{2D_L}{u_{SF}} + 2 \cdot \left(\frac{k'_i}{1 + k'_i} \right)^2 \cdot \frac{1}{k'_i \cdot k_{M,i}} \cdot u_{SF} \tag{10}$$

The lumped axial dispersion coefficient D_L contains contributions of axial molecular diffusion and Eddy diffusion [28]:

$$D_L = \gamma_1 \cdot D_m + \gamma_2 \cdot d_P \cdot u_{SF} \tag{11}$$

where D_m is the molecular diffusion coefficient and γ_1 and γ_2 are numerical parameters. In the flow rate range applied in preparative chromatography, the molecular diffusion term in Eq. (11) is negligible. Consequently, Eq. (11) can be written in the form of a linear function:

$$\mathrm{HETP}\ (u_{SF}) = A + C_S \cdot u_{SF} \tag{12}$$

with

$$A = 2 \cdot \gamma_2 \cdot d_P = 2 \cdot d_{ax} \tag{13}$$

and

$$C_S = 2 \cdot \left(\frac{k'_i}{1 + k'_i} \right)^2 \cdot \frac{1}{k'_i \cdot k_{M,i}} \tag{14}$$

where d_{ax} is the reduced axial dispersion coefficient.

The linear functions obtained through data fitting of the van Deemter plot are now compared to Eq. (12):

Firstly, the reduced axial dispersion coefficient d_{ax} is given according to Eq. (13) by the *y*-axis intercept A divided by 2 of the linear correlation described by Eq. (12). Secondly, the lumped mass transfer coefficient $k_{M,i}$ is calculated according to Eq. (14) from the slope C_S of the linear function described by Eq. (12), taking into account the retention factors k'_i at the different salt concentrations that were investigated. Consequently, the range of $k_{M,i}$ values for the range of the salt concentrations applied during the linear gradient elution of the model validation runs could be estimated. This procedure neglects the dependence of $k_{M,i}$ on the mAb concentration since it uses only information from analytical injections; however, experimental validation shows that $k_{M,i}$ was determined in the correct order of magnitude.

In order to evaluate the saturation capacities $q_{Sat,i}$, experiments under preparative conditions were carried out by loading UF/DF-treated purified mAb onto Fractogel SO_3 (M) and Poros HS 50 columns as described in Section 2. The eluate flows were

Table 1
Mass transfer coefficient $k_{M,mAb}$ and axial dispersion coefficient d_{ax} for Fractogel SO_3 (M) and Poros HS 50 under non-adsorbing (90% B, 60% B) and adsorbing conditions (24% B) at pH 6.0.

	$k_{M,i}$ (1/min)			d_{ax} (cm)		
% Buffer B	90%B	60%B	24%B	90%B	60%B	24%B
NaCl conc.	0.27 M	0.18 M	0.072 M	0.27 M	0.18 M	0.072 M
Fractogel SO_3 (M)	4.8	2.1	0.9	0.19	0.20	0.24
Poros HS50	2.4	3.4	3.2	0.03	0.03	0.07

fractionated and the mAb was quantified by analytical protein A chromatography. The saturation capacities were determined by peak fitting using the lumped kinetic model equations. The peak fitting had to be based on the peak profile obtained from offline protein A analyses since the online UV-monitoring at 280 nm was strongly non-linear during the elution.

The estimated values for all the parameters discussed in this section are summarized in the following.

The results of the Henry coefficient determination are shown as a function of salt concentration in Fig. 2 for Fractogel SO_3 (M) and Poros HS 50 for three different pH values. It is seen that the Henry coefficients of Poros HS 50 are larger than those of Fractogel SO_3 (M) at the investigated pH conditions.

Fig. 3 shows a plot of the plate height as a function of the superficial velocity u_{SF} (van Deemter-plot) with the corresponding fitting straight lines. The estimated values of $k_{M,i}$ and d_{ax} are summarized in Table 1.

Fig. 3 and Table 1 suggest that the change in the mass transfer coefficient from non-adsorbing to adsorbing conditions is much larger for Fractogel SO_3 (M) than for Poros HS 50. This could be attributed to the sensitivity of the stationary phase tentacles structure in the resin pores to the buffer ionic strength, which is obviously present in Fractogel SO_3 (M) and not in Poros HS 50. High salt concentrations would in fact screen the tentacles charges which would the collapse on the pore walls thus leading to larger mass transfer coefficients [38]. While at 90% B, the mass transfer is higher for Fractogel than for Poros, it is lower at 60% B and 24% B. The Poros material, which is claimed to be a "perfusion" material and is therefore expected to have a very high mass transfer coefficient actually exhibits a $k_{M,mAb}$ value which is in the same range as that of the Fractogel material. However, under adsorbing conditions, which are those of interest in gradient chromatography, the Poros material exhibits larger mass transfer coefficients. In subsequent simulations of batch and MCSGP experiments a mass transfer coefficient of $k_{M,mAb} = 1.5\ min^{-1}$ was used in the case of Fractogel SO_3 (M), which represents the mean value between the value determined at 0.072 M (24% B, $k_{M,mAb} = 0.9\ min^{-1}$) and the value determined at 0.18 M (60% B, $k_{M,mAb} = 2.1\ min^{-1}$). Typical gradient conditions for the mAb elution are in fact between 0 and 0.1 M NaCl (pH 6.0). For Poros HS 50, the average lumped mass transfer coefficient of $k_{M,mAb} = 3.3\ min^{-1}$ was used. In analogy, the axial dispersion coefficient d_{ax} was averaged, leading to values of 0.22 cm for Fractogel SO_3 (M) and 0.05 cm for Poros HS 50.

The saturation capacities were estimated by peak fitting as illustrated in Fig. 4. The best fit of the elution profile was obtained with $q_{Sat} = 110$ g/L for Poros HS 50 and with $q_{Sat} = 120$ g/L for Fractogel SO_3 (M).

The Henry coefficient and the saturation capacity for the salt adsorption equilibria are actually lumping together effects such as pH perturbations that occur as a consequence of the change in salt concentration during the gradient elution. They were fitted qualitatively to the conductivity signal of the batch gradient experiments using Eqs. (1) and (2) and the salt adsorption equilibrium equation. The same values for salt adsorption could be adopted for Fractogel SO_3 (M) and Poros HS 50. Note that the mass transfer coefficient for the salt was set high enough to account for the high mobility of the salt ions, due to their small size, so as to achieve local equilibrium conditions. Summarizing, the parameter values listed in Table 2 were used for modeling.

In order to complete the determination of the model parameters, the chromatographic flow velocity u_i is calculated as the ratio between the superficial velocity u_{SF} and the porosity ε_i. The superficial velocity u_{SF} in turn is calculated from the ratio of the volumetric flow rate and the cross section area of the column.

4. Model validation

4.1. Impurities adsorption equilibria and model validation with batch experiments

Single column gradient elutions were carried out using pretreated cCCS as feed material to confirm the model parameters for the mAb estimated above and to evaluate the selectivities for the mAb-related impurities. The outlet streams of the gradient runs were fractionated and analyzed offline with the Propac analysis.

In Fig. 5 results of batch gradient simulations (curves) are compared with the corresponding experimental data (points).

The retention time of the mAb was predicted correctly using the model. Although the mass transfer coefficient $k_{M,i}$ was determined under linear conditions, the mAb peak width was described accurately, indicating that the mAb concentrations are close to the linear range of the isotherm. The impurities data (W1, W2 + W3, and aggregates) were fitted assuming a constant selectivity with respect to the main component (mAb), that is the value of the parameter α_1 in Eq. (8) was fitted for all impurities while that of α_2 in the same equation was kept constant and equal to the corresponding value for the mAb. Since W2 and W3 exhibited very similar elution behavior on the preparative stationary phase, they were treated as a single impurity. The so obtained selectivities are summarized in Tables 3 and 4 along with the isotherm parameters

Table 2
Values of the chromatographic model parameters for Fractogel SO_3 (M) and Poros HS 50.

Model constants		Unit	$FGSO_3$ (M)	Poros HS50	Acquisition method
ε_i	Porosity for mAb and impurities	–	0.5	0.58	Pulse inject., non-ads., isocrat.
ε_{NaCl}	Porosity for salt	–	0.88	0.78	Pulse inject., isocrat.
$d_{ax,mAb}$	Axial dispersion coeff. of mAb	cm	0.2	0.05	van Deemter-plot (mAb)
$d_{ax,W}$	Axial dispersion coeff. of impurities	cm	0.2	0.05	Set same as mAb
$k_{M,mAb}$	Mass transfer coefficient of mAb	1/min	1.5	3.3	van Deemter-plot (mAb)
$k_{M,W}$	Mass transfer coefficient of impurities	1/min	1.5	3.3	Set same as mAb
q_{Sat}	Saturation capacity	g/L	120	110	Overloaded expts., peak-fitting

Table 3
Isotherm parameters in Eqs. (3) and (8) for Fractogel SO_3 (M).

Component	$\alpha_{1,i}$	$\alpha_{2,i}$	$q_{Sat,i}$	Selectivity = $\alpha_{1,i}/\alpha_{1,mAb}$	Estimation method
W1	300	−5.81	120	0.02	Fitted
W2 & W3	1000	−5.81	120	0.07	Fitted
mAb	15 184	−5.81	120	1.00	Pulse inject., isocrat.
S (Agg.)	50 000	−5.81	120	3.29	Fitted
NaCl	2	0	300	n.a.	Fitted

for the pure mAb determined above for Fractogel SO_3 (M) and Poros HS 50, respectively.

Porosities, mass transfer parameters and saturation capacities of W1, W2 + W3 and aggregates were assumed to be the same as the corresponding mAb values.

It has to be noted that the quantitative information on the impurity concentrations shown in Fig. 5 is not complete since the fragment clearance during the loading step is not included (see Section 2.4). In order to fit the concentration profile of W1 and W2 + W3 to the experimental values, the initial fragment concentration had to be reduced by a factor 4 (Fractogel SO_3 (M)) and a factor 15 (Poros HS 50) in the simulation with respect to the analytically determined values.

In summary, we can conclude that with the model parameters determined above the simulation model is capable of accurately predicting the yield and the main component concentration profile in batch processes. It is worth reiterating that the model is of limited use with respect to the determination of absolute purity values since fragment clearance during loading and, more importantly, HCP content, are not sufficiently quantified. However, the fitted selectivities of W1, W2 + W3 and aggregates, allow for relative comparisons of the purity values among simulations for a single resin at constant feed conditions. Considering the inherent complexity of the considered system this has to be regarded as a satisfactory result for a simulation model.

4.2. MCSGP model validation with experimental runs

The model developed above has been used in this work to confirm the design of the operating conditions of the MCSGP process. The experimental operating parameter determination procedure [32] provided initial values for the simulations. In the simulations, the operating parameters (more precisely the flow rates in zones 2 and 4) were fine-tuned so that a yield of >95% was predicted. In addition, the model was used to carry out robustness analyses of the operating points. A summary of the final operating parameters is given in Table S-I in the supplementary material section of [10]. In this section we compare model predictions and experimental results for three MCSGP runs, reported by Muller-Spath et al. [10], in terms of the product concentration and the yield, which are closely related. In particular, we will consider not only cyclic steady state conditions, but also the start-up and the shutdown phases.

During the start-up phase, mAb is accumulated in the MCSGP unit until the cyclic steady state is reached. Thus, the calculated product concentrations and yields (fraction of purified product leaving the unit with respect to the product in the feed) increase from zero to their steady state values. At cyclic steady state, the cycle-average product outlet concentration and yield remain constant over time. During the shutdown phase, the feeding of cCCS is replaced by a feeding with buffer A. Nevertheless, based on the feed concentration during steady state operation an apparent yield can be determined which is decreasing over time as the mAb is eluted from the MCSGP unit. However, due to the feeding with buffer A the product purity remains high in this phase.

It has to be noted that the simulation of the purity does not include HCP and fragment clearance during the loading step and can therefore serve only as a relative performance parameter for comparison between the simulations of the different MCSGP experiments.

Fig. 6 shows the startup and the steady state phase of run MCSGP 1 (Fractogel SO_3 (M)). The results from offline protein A analytics, i.e. the mAb concentration, the yield and the purity, are compared to the simulation results as a function of time. The bars and vertical dashed lines stand for the duration of the sample collection for offline-analyses. The performance parameters represent average values over these intervals both in offline measurements and simulations. During the startup phase, which is in this case completed basically after two cycles (cycle duration is 64 min in run MCSGP 1 and 40 min in runs MCSGP 2 & 3), the average product concentration, yield and purity values of the first cycle are 1.2 g/L, 42.9% and 96.9%, respectively, according to offline analyses. Simulations predicted 1.0 g/L, 55.7% and 99.1%, respectively. The values of the second cycle are 2.4 g/L, 83.3% and 97.4%, respectively, according to offline analyses while simulations predicted 2.8 g/L, 99.3% and 99.0%, respectively.

Experimentally, cyclic steady state is confirmed by comparing the repetitive pattern of the UV signal of the product elution peaks between the cycles (four product elution peaks per cycle, since four columns are used). Run MCSGP 1 reaches the cyclic steady state yield and purity values of 94.9% and 97.4%, respectively and an average product pool concentration of 2.8 g/L. Simulations predicted 99.6% yield, 99.0% purity and 2.8 g/L mAb concentration.

For run MCSGP 2 (Poros HS 50), shown in Fig. 7, steady state is basically reached within one cycle due to an increased feed flow rate leading to a faster accumulation of mAb in the MCSGP unit.

The values of the startup cycle for concentration, yield and purity are 2.7 g/L, 56.7% and 98.6%, respectively, according to offline analyses. The simulations predicted 2.4 g/L, 61.4% and 97.7%, respectively.

According to the offline protein A analyses, at cyclic steady state, the mAb concentration reaches 4.7 g/L, corresponding to a yield of 96.1% at a product purity of 97.5%. The simulation predicted a concentration of 4.5 g/L and yield and purity values of 97.2% and 96.7%, respectively.

Table 4
Isotherm parameters in Eqs. (3) and (8) for Poros HS 50.

Component	$\alpha_{1,i}$	$\alpha_{2,i}$	$q_{Sat,i}$	Selectivity = $\alpha_{1,i}/\alpha_{1,mAb}$	Estimation method
W1	1900	−6.34	110	0.02	Fitted
W2 & W3	6600	−6.34	110	0.07	Fitted
mAb	94 708	−6.34	110	1.00	Pulse inject., isocrat.
S (Agg.)	312 000	−6.34	110	3.29	Fitted
NaCl	2	0	300	n.a.	Fitted

Table 5
Summary of MCSGP performance according to experiments and model simulations.

Run MCSGP	Yield (%)		Mass bal. closure (%)		Product purity (%)		mAb conc. in product stream (g/L)		Productivity (g/L/h)	
	Exp.	Sim.	Exp.	Sim.	Exp.	Sim.	Exp.	Sim.	Exp.	Sim.
MCSGP1	94.9	99.6	98.6	100.0	97.4	99.0	2.7	2.8	6	6
MCSGP2	96.1	97.2	100.1	100.0	97.5	96.6	4.7	4.5	24	23
MCSGP3	96.0	97.2	100.8	100.0	96.9	94.6	4.9	4.9	25	25

Run MCSGP	mAb conc. in feed (g/L)	Feed purity (%)	HCP in product stream (ppm)	HCP clearance (*x*-fold)	u_{load} (cm/h)	Buffer Cons.	
						wo dil (L/g) Exp.	w dil (L/g) Exp.
MCSGP1	0.45	21.1	146	1027	550	1.6	3.4
MCSGP2	0.51	21.1	226	664	2000	0.9	2.2
MCSGP3	0.70	21.1	625	240	1500	0.8	1.8

During the shutdown phase the concentration and the yield decrease rapidly as no more mAb is fed to the system, but the product collected over the first cycle of the shutdown phase still has a purity of 96.6% and the purity of the second cycle of the shutdown phase, where the product concentration becomes negligible, is still 93%. The overall yield of the process excluding the last cycle, which is too low in purity (<95%), is calculated from the total mass of mAb fed to the system and the mAb mass in the product outlet in specification. An experimental value of 95.7% and a simulated value of 94.9% are obtained for the overall yield.

In run MCSGP 3, shown in Fig. 8 at cyclic steady state, according to offline analytics values of 4.7 g/L, 96.1% and 97.5% are reached for concentration, yield and purity, respectively. Results from simulations were 4.5 g/L, 97.2% and 94.6%, for concentration, yield and purity, respectively.

The productivity values of MCSGP 1, 2 and 3 were 6 g/L/h, 24 g/L/h and 25 g/L/h, respectively, at cyclic steady state. These correspond well with the computed values of 6, 23 g/L/h and 25 g/L/h, respectively.

From the data in Figs. 6–8 it can be concluded that the startup and steady state product concentrations predicted by the simulations are in very good agreement with the experimental data. For run MCSGP 1 the product concentration is overpredicted by 3%, while for run MCSGP 2 it is underpredicted by ca. 5% and for run MCSGP 3 the deviation is smaller. In run MCSGP 1, the yield is overpredicted by 5% as a consequence of the overprediction of the concentration. In runs MCSGP 2 and 3 the yield differs by 1–2%. The smaller deviation can be possibly attributed to a more accurate determination of the model parameters for Poros HS 50.

The performance results of the runs MCSGP 1 (Fractogel SO_3 (M)), MCSGP 2 and MCSGP 3 (both Poros HS 50) are summarized in Table 5.

The reported values for yield, purity, concentrations and mass balance closure were calculated from the mAb concentrations obtained from the offline protein A analysis and the flow rates. Two values of the buffer consumption per unit mass of purified mAb are reported: one corresponds to the actual process where the feed is diluted (denoted by "w dil") and the other to a hypothetical process (denoted by "wo dil") where the feed would not need to be diluted and the supernatant could be fed as such to the MCSGP unit. Furthermore, in the same table, the mAb concentration in the feed and product streams, the HCP concentration and clearance ratio in the product stream and the productivity, in terms of grams of purified mAb per unit of time and volume of column are reported. ELISA results show that with both materials, Fractogel SO_3 (M) and Poros HS 50, it is possible to reach a yield of 95% with HCP-contents between 100 and 700 ppm. Further aspects of these results and a comparison with the batch gradient process have been discussed by Muller-Spath et al. [10].

5. Conclusion

A cation exchange capture step for a monoclonal antibody from cell culture supernatant by batch and continuous chromatography was modeled using a lumped kinetic model.

A procedure for determining all the model parameters was developed and demonstrated for two cation exchange stationary phases. The procedure comprises retention measurements under analytical conditions at varying flow rates to determine retention factors and mass transfer parameters of the product component, i.e. the mAb, alone. Moreover, peak fitting is carried out using data from overloaded experiments in order to determine saturation capacities.

The procedure is easily implementable using only single column batch experiments and requires relatively small amounts of purified feed material.

Using batch experiments with the cell culture supernatant, it was possible to validate the model results with respect to the mAb and to simultaneously estimate the selectivities of all the relevant impurities and to provide starting values for MCSGP simulations. Subsequently the model was used to predict the performance of the continuous MCSGP process in terms of product concentration and yield. With regard to product yield and concentration, the presented model has proved to predict the performance with high accuracy (error $\leq$ 6%), making it a very useful tool in process development. The productivities achieved in the model validation runs were in an industrially relevant range with values up to 25 g mAb/L of stationary phase per hour.

It is worth noting that the developed model does not provide quantitative information about product purities, since suitable analytics for HCP were not available.

Nomenclature

c_1–c_4, c_6	gradient concentrations (g/L)
c_i	concentration of component i (g/L)
c_{feed}	feed concentration (g/L)
d_{ax}	axial dispersion coefficient (cm)
d_p	particle diameter (μm)
V_C	column volume (mL)
F	phase ratio $F = (1-\varepsilon)/\varepsilon$ (–)
H_i	Henry coefficient for component i (–)
k'_i	retention factor, component i (–)
$k_{M,i}$	lumped mass transfer coefficient, component i (1/min)
mAb	monoclonal antibody (–)
q_i	solid phase concentration of component i (g/L)
q_i^*	solid phase equilibrium concentration of component i (g/L)

$q_{Sat,i}$ saturation capacity for component i (g/L)
Q flow rate (mL/min)
Q_1–Q_4, Q_6 flow rates for the sections 1–4, 6 of the MCSGP process (mL/min)
Q_{CIP} flow rate of CIP step (mL/min)
Q_{Equil} flow rate of equilibration step (mL/min)
Q_{Feed} feed flow rate for MCSGP process (mL/min)
t_{BL} time period length of MCSGP batch state (min)
t_{CC} time period length of MCSGP interconnected state (min)
t_0 retention time under non-adsorbing conditions (min)
t_{run} total batch experiment run time (min)
t_p injection time endpoint (min)
$t_{R,i}$ retention time, component i (min)
u_i chromatographic mobile phase velocity (cm/h)
u_{SF} superficial mobile phase velocity (cm/h)
$\alpha_{1,i}$ empirical constant for Henry function, component i (–)
$\alpha_{2,i}$ empirical constant for Henry function, component i (–)
ε_i specific porosity for component i (–)

References

[1] A. Beck, T. Wurch, C. Bailly, N. Corvaia, Nat. Rev. Immunol. 10 (2010) 345.
[2] S. Aggarwal, Nat. Biotechnol. 28 (2010) 1165.
[3] A.A. Shukla, J. Thommes, Trends Biotechnol. 28 (2010) 253.
[4] B. Kelley, Biotechnol. Prog. 23 (2007) 995.
[5] G.M. Ferreira, J. Dembecki, K. Patel, A. Arunakumari, Biopharm. Int. 20 (2007) 32.
[6] M. Urmann, H. Graalfs, M. Joehnck, L.R. Jacob, C. Frech, Mabs 2 (2010) 395.
[7] T. Muller-Spath, L. Aumann, M. Morbidelli, Sep. Sci. Technol. 44 (2009) 1.
[8] A. Stein, A. Kiesewetter, J. Chromatogr. B: Anal. Technol. Biomed. Life Sci. 848 (2007) 151.
[9] A. Mehta, M.L. Tse, J. Fogle, A. Len, R. Shrestha, N. Fontes, B. Lebreton, B. Wolk, R. van Reis, Chem. Eng. Prog. 104 (2008) S14.
[10] T. Muller-Spath, L. Aumann, G. Strohlein, H. Kornmann, P. Valax, L. Delegrange, E. Charbaut, G. Baer, A. Lamproye, M. Johnck, M. Schulte, M. Morbidelli, Biotechnol. Bioeng. 107 (2010) 974.
[11] J. Wang, T. Diehl, D. Aguiar, X.P. Dai, A. Arunakumari, Biopharm. Int. (2009) 4.
[12] T. Peram, P. McDonald, J. Carter-Franklin, R. Fahrner, Biotechnol. Prog. 26 (2010) 1322.
[13] T. Yang, M.C. Sundling, A.S. Freed, C.M. Breneman, S.M. Cramer, Anal. Chem. (Washington, DC, US) 79 (2007) 8927.
[14] A. Ladiwala, K. Rege, C.M. Breneman, S.M. Cramer, Proc. Natl. Acad. Sci. U. S. A. 102 (2005) 11710.
[15] B. Guelat, G. Strohlein, M. Lattuada, M. Morbidelli, J. Chromatogr. A 1217 (2010) 5610.
[16] A.M. Lenhoff, Langmuir 24 (2008) 5991.
[17] M.C. Stone, G. Carta, J. Chromatogr. A 1160 (2007) 206.
[18] A.L. Zydney, C. Harinarayan, R. van Reis, Biotechnol. Bioeng. 102 (2009) 1131.
[19] S.R. Dziennik, E.B. Belcher, G.A. Barker, M.J. DeBergalis, S.E. Fernandez, A.M. Lenhoff, Proc. Natl. Acad. Sci. U. S. A. 100 (2003) 420.
[20] N. Forrer, A. Butte, M. Morbidelli, J. Chromatogr. A 1214 (2008) 71.
[21] C.A. Orellana, C. Shene, J.A. Asenjo, Biotechnol. Bioeng. 104 (2009) 572.
[22] C.A. Brooks, S.M. Cramer, AIChE J. 38 (1992) 1969.
[23] S.R. Gallant, S. Vunnum, S.M. Cramer, AIChE J. 42 (1996) 2511.
[24] D. Ruthven, Principles of Adsorption and Adsorption Processes, John Wiley & Sons, Inc., New York, 1984.
[25] A. Voitl, A. Butte, M. Morbidelli, J. Chromatogr. A 1217 (2010) 5492.
[26] M. Degerman, N. Jakobsson, B. Nilsson, J. Chromatogr. A 1113 (2006) 92.
[27] G. Guiochon, S. Golshan-Shirazi, AM. Katti, Fundamentals of Preparative and Nonlinear Chromatography, Academic Press, Boston, 1994.
[28] K. Miyabe, G. Guiochon, J. Chromatogr. A 890 (2000) 211.
[29] A. Seidel-Morgenstern, J. Chromatogr. A 1037 (2004) 255.
[30] G. Carta, A.R. Ubiera, T.M. Pabst, Chem. Eng. Technol. 28 (2005) 1252.
[31] L. Aumann, M. Morbidelli, Biotechnol. Bioeng. 99 (2008) 728.
[32] L. Aumann, M. Morbidelli, Biotechnol. Bioeng. 98 (2007) 1043.
[33] L. Aumann, G. Stroehlein, M. Morbidelli, Biotechnol. Bioeng. 98 (2007) 1029.
[34] T. Muller-Spath, L. Aumann, L. Melter, G. Strohlein, M. Morbidelli, Biotechnol. Bioeng. 100 (2008) 1166.
[35] T. Muller-Spath, M. Krattli, L. Aumann, G. Strohlein, M. Morbidelli, Biotechnol. Bioeng. 107 (2010) 652.
[36] P. Barker, Preparative and Production Scale Chromatography, Marcel Dekker, New York, Basel, Hong Kong, 1993.
[37] J.J. van Deemter, F.J. Zuiderweg, A. Klinkenberg, Chem. Eng. Sci. 5 (1956).
[38] N. Forrer, O. Kartachova, A. Butte, M. Morbidelli, Ind. Eng. Chem. Res. 47 (2008) 9133.